

Nonconvex models for recovering images corrupted by salt-and-pepper noise on surfaces

Yuan Liu ^{*} Peiqi Yu [†] Chao Zeng [‡]

Abstract *Image processing on surfaces has drawn significant interest in recent years, particularly in the context of denoising. Salt-and-pepper noise is a special type of noise which randomly sets a portion of the image pixels to the minimum or maximum intensity while keeping the others unaffected. In this paper, We propose the L_p TV models on triangle meshes to recover images corrupted by salt-and-pepper noise on surfaces. We establish a lower bound for data fitting term of the recovered image. Motivated by the lower bound property, we propose the corresponding algorithm based on the proximal linearization method with the support shrinking strategy. The global convergence of the proposed algorithm is demonstrated. Numerical examples are given to show good performance of the algorithm.*

Keywords image on surface, image denoising, salt-and-pepper noise, variational methods, nonconvex optimization

Mathematics Subject Classifications (2010)

1 Introduction

Image processing on surface is widely used in computer vision [18], computer graphics[4], and medical imaging [28]. To generate an image on a surface, we need to transform an image defined on a surface into a point cloud by sampling specific points, each associated with a pixel value. Subsequently, a triangle mesh is constructed from this point cloud, where each vertex corresponds to a pixel value, as illustrated in Figure 1. The pixel values at arbitrary points on the triangle mesh are estimated by interpolation. There is still a relative scarcity of research in image processing on surface. Current work includes methods based on partial differential equations [5, 31] and, more commonly, variational approaches. For example, variational methods based image segmentation is discussed in [12, 17] and image decomposition is considered in [16, 34].

When the data are gathered, errors may be introduced by measurement tools, processing or by experts. These errors are called noise. For an image on surface, errors may be introduced when sampling. That is, the pixel values at the vertices of a triangle mesh may be corrupted by noise. Denoising is a fundamental challenge in image processing. Various denoising techniques have been proposed in the literature. In the context of 2D images, among the methods employed for image denoising are filtering techniques, PDEs-based methods, wavelet-based approaches, and variational methods. Variational methods, in particular, focus on recovering 2D images by solving optimization models that promote gradient sparsity. In recent years, nonconvex and nonsmooth variational methods have gained prominence [6, 14, 24, 25] due to their remarkable advantages over convex and smooth variational methods, particularly in edge-preserving image restoration. These methods are especially effective in restoring high-quality, piecewise constant images with neat edges [22, 37]. Despite their advantages, designing efficient algorithms for nonconvex models remains a challenging task. Surface image denoising presents significantly greater challenges compared to

^{*}School of Mathematics, Hefei University of Technology, Hefei, China. E-mail: liuyzz@hfut.edu.cn. Y. Liu’s research is supported in part by the National Natural Science Foundation of China (No. 62002095).

[†]School of Mathematical Sciences and LPMC, Nankai University, Tianjin, China. E-mail: 2120220074@mail.nankai.edu.cn.

[‡]Corresponding author. School of Mathematical Sciences and LPMC, Nankai University, Tianjin, China. E-mail: zengchao@nankai.edu.cn. C. Zeng’s research is supported in part by the National Natural Science Foundation of China (No. 12201319) and the Fundamental Research Funds for the Central Universities, Nankai University (No. 63231142).

2D image denoising, as effective denoising in this context requires careful consideration of both the data set and the underlying mesh structure. Researches on image denoising techniques for triangle meshes are few in the existing literature, with only a few studies addressing this topic [13, 20, 21, 30, 31, 33]. Among these, the works of [30, 31] employ PDE-based methods, with [31] focusing on a full scale-space analysis. In contrast, studies [13, 20, 21, 33] adopt variational methods, where an analogy to the total variation (TV) model [27] on surfaces is proposed and examined. A central challenge in these approaches is the definition of a discrete gradient for data sets on triangle meshes. A commonly adopted strategy is to interpolate the discrete data set over the mesh, thereby enabling the definition of the discrete gradient through the interpolation function. Linear interpolation is predominantly used in studies [20, 21, 30, 31, 33], while [13] employs Raviart-Thomas basis functions for interpolation.

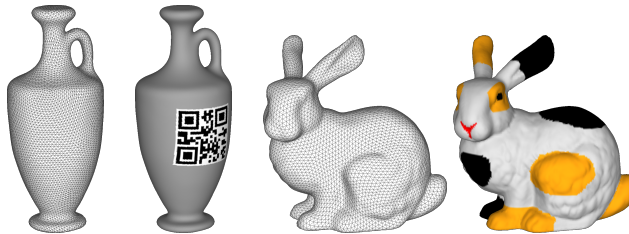


Figure 1: Triangle meshes and images on triangle meshes.

Unlike many papers focusing on gaussian noise, in this paper, we consider recovering images on surface corrupted by salt-and-pepper noise. This kind of noise is usually caused by sudden disturbances in image acquisition, such as errors in data transmission, faulty sensors, or analog-to-digital conversion errors. In an image with salt-and-pepper noise, some pixels are randomly set to the minimum (black) or maximum (white) intensity, while others remain unaffected. For 8 bits images, all pixels of the original image \underline{u} range from 0 to 255, i.e., $0 \leq \underline{u}_j \leq 255$, for all j . Then, for the observed data f corrupted by salt-and-pepper noise with noise level ρ , we have

$$|\underline{u}_j - f_j| = \begin{cases} |0 - \underline{u}_j|, & \text{with probability } \frac{\rho}{2}; \\ |255 - \underline{u}_j|, & \text{with probability } \frac{\rho}{2}; \\ 0, & \text{with probability } 1 - \rho. \end{cases} \quad (1)$$

It is clear that the restoration of \underline{u} from the data corrupted by salt-and-pepper noise has the demand of sparse reconstruction of the data fitting term: $(1 - \rho)$ percent of entries of the data fitting term with the true solution \underline{u} are zero for noise level ρ .

From the perspective of sparse reconstruction, ℓ_0 data fitting term is a natural choice, but it is an NP-hard problem. Instead, in 2D image processing, the most general alternative is the ℓ_1 data fitting term [11, 23, 35]. The ℓ_p minimization has advantages over the ℓ_1 minimization in sparse reconstruction; see [10, 19, 21, 22, 37]. Hence, it is reasonable to consider using the ℓ_p minimization for the data fitting term. Consequently, we consider image denoising on triangle meshes with nonconvex variational method. We utilize linear interpolation like [20]. We propose the L_p TV model on triangle meshes. Based on the corresponding lower bound property of the model, we adopt the proximal linearization method (PLM). Every subproblem can be solved by the alternating direction method of multipliers (ADMM). We obtain the global convergence of the PLM. The efficiency of the propose method is illustrated by related numerical experiments.

The rest of this paper is organized as follows. In Section 2, we introduce basic definitions for images on triangle meshes. In Section 3, we present the models, establish a lower bound for the data fitting term of local minimizers, and propose the corresponding algorithm. The convergence analysis are given in Section 4. Applications are given in Section 5. Conclusions are presented in Section 6.

Notation

For a real-valued matrix G , G^\top is its transpose, and $\|G\|$ is its spectral norm. For two vectors $g, h \in \mathbb{R}^r$, the inner product of the two vectors is $\langle g, h \rangle = g^\top h$, and the ℓ_2 norm of g is $\|g\|$. Denote by e_j the column vector whose j th component is one while all the others are zeros. For a real number r , the signum function $\text{sgn}(r)$ is defined as

$$\text{sgn}(r) = \begin{cases} -1, & \text{if } r < 0; \\ 0, & \text{if } r = 0; \\ 1, & \text{if } r > 0. \end{cases}$$

The exact notation and definition of subdifferential can be found in Appendix A

2 Preliminaries

We introduce the discretization of surfaces and images on surfaces. These techniques can be found in [15, 16, 31].

2.1 Triangulated surfaces

A connected surface in \mathbb{R}^3 can be approximated by a triangle mesh. Assume that Δ is a triangle mesh in \mathbb{R}^3 with no degenerate triangles. The set of the indices of all vertices and the set of the indices of all triangles of Δ are denoted by I_v and I_τ , respectively. Then, the set of vertices and the set of triangles of Δ are denoted as $\{v_i : i \in I_v\}$, and $\{\tau_i : i \in I_\tau\}$, respectively. The numbers of vertices and triangles are denoted by N_v and N_τ , respectively. A triangle whose vertices are v_i, v_j, v_k is denoted as $[v_i, v_j, v_k]$. The area of a triangle τ is denoted by $|\tau|$.

For a vertex v , we define the *star* of v , denoted by $\text{star}(v)$, to be the set of all triangles in Δ which share the vertex v . For the mesh Δ , the *dual mesh* is formed by connecting the barycenter and the middle point of each edge in each triangle. As illustrated in Figure 2, the original mesh Δ consists of black lines, while the dual mesh is in red. The *control cell* of a vertex v_i is part of its star which is near to v_i in the dual mesh. Figure 2 shows the control cell C_i for an interior vertex v_i of the original mesh and the control cell C_j for a boundary vertex v_j . See [15, 31] for more details.

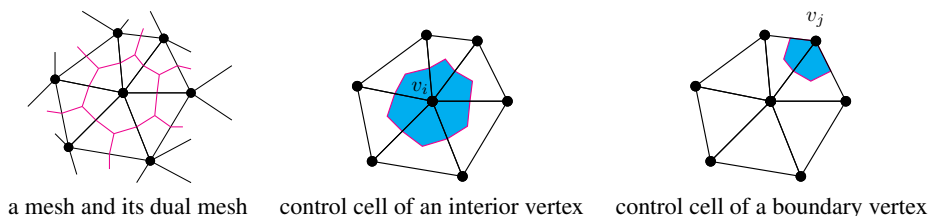


Figure 2: Dual mesh and control cells.

2.2 Discretization of images on surfaces

A grayscale image on the triangulated surface Δ is a function $u : \Delta \rightarrow \mathbb{R}$ with $u(x)$ being the pixel value of the point x on Δ . The image u is sampled over the vertices of the mesh and the value $u(x)$ at any point x on Δ is estimated by linear interpolation. That is, u is understood as a piecewise linear function.

Let

$$u_i := u(v_i), \quad i = 1, 2, \dots, N_v,$$

and let $u = [u_1, u_2, \dots, u_{N_v}]^\top \in \mathbb{R}^{N_v}$. Denote the piecewise linear space by

$$\mathcal{L}(\Delta) := \{u \in C^0(\Delta) : u|_{\tau_i} \in \mathbb{P}_1, i \in I_\tau\},$$

where \mathbb{P}_1 denotes the space of trivariate linear polynomials. For each vertex v_i , we use ϕ_i to denote the piecewise linear function with support on $\text{star}(v_i)$, i.e.,

$$\phi_i \in \mathcal{L}(\Delta) \text{ and } \phi_i(v_j) = \delta_{ij}, \quad i, j \in I_v,$$

where δ_{ij} is the Kronecker delta. Then $\{\phi_i : i = 1, \dots, N_v\}$ forms a basis of $\mathcal{L}(\Delta)$. The function obtained by linear interpolation is

$$\mathbf{u}(x) = \sum_{i \in I_v} u_i \phi_i(x). \quad (2)$$

Since \mathbf{u} is determined by u , for convenience, we also call u an image on surface.

By [31, (4.2)], we have

$$\int_{\Delta} \mathbf{u} \, dx = \sum_{\tau=[v_l, v_m, v_n]} \frac{|\tau|}{3} (u_l + u_m + u_n) = \sum_{i \in I_v} u_i \sum_{\tau \in \text{star}(v_i)} \frac{|\tau|}{3} = \sum_{i \in I_v} u_i s_i,$$

where s_i is the area of the control cell of the vertex v_i . The discrete gradient of u can be defined by the gradient of u . Since u is only C^0 on Δ , we consider the gradient of u on every triangle

$$\nabla \mathbf{u}|_{\tau} = \sum_{i \in I_v} u_i \nabla \phi_i|_{\tau}.$$

The calculation of $\nabla \phi_i|_{\tau}$ is given in [31] by using the natural piecewise parametrization. See Figure 3, where O is the Euclidean projection of v_i on the line passing through v_j, v_k .

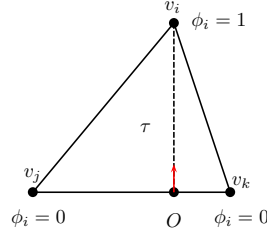


Figure 3: The gradient of the basis ϕ_i restricted on $[v_i, v_j, v_k]$: the red vector.

Denoting $h_i^{\tau} = v_i - O$ (see the red vector in Figure 3), the deduction in [31] shows that the gradient of ϕ_i restricted on $\tau = [v_i, v_j, v_k]$ is

$$\nabla \phi_i|_{[v_i, v_j, v_k]} = \frac{h_i^{\tau}}{|h_i^{\tau}|^2}.$$

As one can see, $\nabla \phi_i|_{\tau}$ is a constant vector, and thus so is $\nabla \mathbf{u}|_{\tau}$:

$$\nabla \mathbf{u}|_{\tau=[v_i, v_j, v_k]} = \frac{u_i h_i^{\tau}}{|h_i^{\tau}|^2} + \frac{u_j h_j^{\tau}}{|h_j^{\tau}|^2} + \frac{u_k h_k^{\tau}}{|h_k^{\tau}|^2}. \quad (3)$$

The discrete gradient operator is defined as

$$D : \mathbb{R}^{N_v} \longrightarrow \mathbb{R}^{3 \times N_{\tau}} \\ u \longmapsto (\nabla \mathbf{u}|_{\tau_1}, \dots, \nabla \mathbf{u}|_{\tau_{N_{\tau}}}).$$

We denote by $D_i u$ the i th column of Du , i.e.,

$$D_i \in \mathbb{R}^{3 \times N_v}, \quad D_i u = \nabla \mathbf{u}|_{\tau_i}. \quad (4)$$

Suppose $\tau_i = [v_{i_1}, v_{i_2}, v_{i_3}]$. By (3), the i_1 th column, the i_2 th column and the i_3 th column of D_i are $\frac{h_{i_1}^{\tau_i}}{|h_{i_1}^{\tau_i}|^2}$, $\frac{h_{i_2}^{\tau_i}}{|h_{i_2}^{\tau_i}|^2}$, $\frac{h_{i_3}^{\tau_i}}{|h_{i_3}^{\tau_i}|^2}$, respectively, and the other entries of D_i are zero.

3 Models and algorithm

We consider the restoration of an image corrupted by impulse noise:

$$f = \underline{u} + n,$$

where f is the observed image, \underline{u} is the original image, and n is the impulse noise. The impulse noise corrupts a portion of elements of \underline{u} while keeping the other elements unaffected. That is, many elements of $\underline{u} - f$ are zero. Suppose \underline{u} is the linear interpolation function of \underline{u} defined in (2). Like 2D images, we know that the norms of the gradient $|\nabla \underline{u}|$ are sparse. Therefore, we can use the idea of sparse reconstruction to restore the original image.

We propose the following L_p TV model:

$$\min_{\underline{u} \in \mathcal{L}(\Delta)} \lambda \sum_{j \in I_v} |u_j - f_j|^p + \int_{\Delta} |\nabla \underline{u}| \, dx, \quad (5)$$

where $\lambda > 0$ is a parameter and $0 < p < 1$. With the symbols introduced in Section 2.2, the discrete version of (5) is

$$\min_{\underline{u} \in \mathbb{R}^{N_v}} \mathcal{F}(u) := \lambda \sum_{j \in I_v} |u_j - f_j|^p + \sum_{i \in I_\tau} |\tau_i| \|D_i u\|, \quad (6)$$

where D_i is defined in (4). Obviously, $\mathcal{F}(u)$ is coercive. Hence, the solution of (6) always exists.

3.1 Lower bound theory

Definition 3.1. For any $u \in \mathbb{R}^{N_v}$, we define the support of the data fitting term as

$$\text{supp}(u) = \{j \in I_v : u_j - f_j \neq 0\}.$$

We have the following lower bound theory for L_p TV model on triangle meshes.

Theorem 3.2. For any local minimizer u^* of $\mathcal{F}(u)$ in (6), there exists a constant $\theta > 0$ such that for all $j \in I_v$, if $|u_j - f_j| \neq 0$, then

$$|u_j^* - f_j| > \theta.$$

Proof. For the local minimizer u^* of $\mathcal{F}(u)$, define the following function

$$\widehat{\mathcal{F}}(u) := \lambda \sum_{j \in \text{supp}(u^*)} |u_j - f_j|^p + \sum_{i \in I_\tau} |\tau_i| \|D_i u\|,$$

and the affine set

$$C := \{v \in \mathbb{R}^{N_v} : v_j = f_j \ \forall j \in I_v \setminus \text{supp}(u^*)\}.$$

It is easy to find that

$$u \in C \quad \Rightarrow \quad \widehat{\mathcal{F}}(u) = \mathcal{F}(u).$$

Because u^* is a local minimizer of $\mathcal{F}(u)$, u^* is a local minimizer of $\widehat{\mathcal{F}}(u)$ over C . The corresponding tangent cone of C is

$$T_C := \{v \in \mathbb{R}^{N_v} : v_j = 0 \ \forall j \in I_v \setminus \text{supp}(u^*)\}.$$

By noticing that T_C is a linear space, the first order optimality condition tells us that there exists $\hat{v} \in \partial \widehat{\mathcal{F}}(u^*)$ such that

$$\langle \hat{v}, u \rangle = 0 \quad \forall u \in T_C. \quad (7)$$

By [26, Exercise 8.8] and [26, Corollary 10.9], we have

$$\partial \widehat{\mathcal{F}}(u^*) = \lambda p \sum_{j \in \text{supp}(u^*)} |u_j^* - f_j|^{p-1} \text{sgn}(u_j^* - f_j) e_j + \partial \left(\sum_{i \in I_\tau} |\tau_i| \|D_i u^*\| \right)$$

$$\begin{aligned}
&= \lambda p \sum_{j \in \text{supp}(u^*)} |u_j^* - f_j|^{p-1} \text{sgn}(u_j^* - f_j) e_j + \sum_{i \in I_\tau} \partial(|\tau_i| \|D_i u^*\|) \\
&\subseteq \lambda p \sum_{j \in \text{supp}(u^*)} |u_j^* - f_j|^{p-1} \text{sgn}(u_j^* - f_j) e_j + \sum_{i \in I_\tau} \{|\tau_i| D_i^\top w_i : \|w_i\| \leq 1, w_i \in \mathbb{R}^3\}.
\end{aligned}$$

By (7), there exists $\bar{w}_i \in \mathbb{R}^3$ satisfying $\|\bar{w}_i\| \leq 1 \forall i \in I_\tau$ such that for any $u \in T_C$, we have

$$\lambda p \sum_{j \in \text{supp}(u^*)} |u_j^* - f_j|^{p-1} \text{sgn}(u_j^* - f_j) u_j = - \sum_{i \in I_\tau} |\tau_i| \langle \bar{w}_i, D_i u \rangle \leq \sum_{i \in I_\tau} |\tau_i| \|D_i\| \|u\|. \quad (8)$$

For every $j \in \text{supp}(u^*)$, let $v^j \in \mathbb{R}^{N_v}$ be the solution to the problem

$$\begin{aligned}
&\min_{v \in \mathbb{R}^{N_v}} \|v\| \\
&\text{s.t. } v \in T_C, \\
&\quad v_j = \text{sgn}(u_j^* - f_j), \\
&\quad \text{sgn}(u_k^* - f_k) v_k \geq 0 \quad \forall k \in \text{supp}(u^*) \setminus \{j\}.
\end{aligned} \quad (9)$$

Since the objective function represents the distance between the origin and the feasible set, and noticing that the feasible set is closed, it follows that (9) is solvable. Define

$$\mu = \max_{j \in \text{supp}(u^*)} \{\|v^j\|\}$$

For a fixed $\bar{j} \in \text{supp}(u^*)$, letting $u = v^{\bar{j}}$ that satisfies (9) and substituting it into (8), we have

$$\begin{aligned}
\lambda p |u_{\bar{j}}^* - f_{\bar{j}}|^{p-1} &= \lambda p |u_{\bar{j}}^* - f_{\bar{j}}|^{p-1} \text{sgn}(u_{\bar{j}}^* - f_{\bar{j}}) v_{\bar{j}}^{\bar{j}} \\
&\leq \lambda p \sum_{j \in \text{supp}(u^*)} |u_j^* - f_j|^{p-1} \text{sgn}(u_j^* - f_j) v_j^{\bar{j}} \\
&\stackrel{(8)}{\leq} \sum_{i \in I_\tau} |\tau_i| \|D_i\| \|v^{\bar{j}}\| \leq \mu \sum_{i \in I_\tau} |\tau_i| \|D_i\|.
\end{aligned}$$

So for every $j \in \text{supp}(u^*)$, we have

$$|u_j^* - f_j|^{p-1} \leq \frac{\mu \sum_{i \in I_\tau} |\tau_i| \|D_i\|}{\lambda p}.$$

Define

$$\theta := \left(\frac{\mu \sum_{i \in I_\tau} |\tau_i| \|D_i\|}{\lambda p} \right)^{\frac{1}{p-1}}. \quad (10)$$

Then, $|u_j^* - f_j| > \theta$ for every $j \in \text{supp}(u^*)$. \square

Corollary 3.3. *Suppose u^* is a local minimizer of $\mathcal{F}(u)$ in (6). Let θ be the lower bound defined in Theorem 3.2. Suppose \hat{u} is a point close to u^* satisfying $|u_j^* - \hat{u}_j| < \theta \quad \forall j \in I_v$. If $|\hat{u}_j - f_j| = 0$ for some $j \in I_v$, then $|u_j^* - f_j| = 0$.*

Proof. If $|\hat{u}_j - f_j| = 0$, by the triangle inequality, we have

$$|u_j^* - f_j| \leq |u_j^* - \hat{u}_j| + |\hat{u}_j - f_j| < \theta.$$

Then by Theorem 3.2, we have $|u_j^* - f_j| = 0$. \square

3.2 Algorithm

In this section, we propose an algorithm based on the theories given in the previous section. Suppose we use an iterative algorithm to find a minimizer u^* of (6) and the iterate sequence is u^k . By Corollary 3.3, if $\lim_{k \rightarrow \infty} u^k = u^*$, there is a k_0 such that

$$\text{if } |u_j^k - f_j| = 0 \text{ for some } k \geq k_0 \text{ and some } j \in I_v \Rightarrow |u_j^* - f_j| = 0.$$

Motivated by this observation, we consider solving u^{k+1} by

$$\begin{cases} \min_{u \in \mathbb{R}^{N_v}} & \lambda \sum_{j \in \text{supp}(u^k)} |u_j - f_j|^p + \sum_{i \in I_\tau} |\tau_i| \|D_i u\|, \\ \text{s.t.} & u_j = f_j \quad \forall j \in I_v \setminus \text{supp}(u^k), \end{cases} \quad (11)$$

where $\text{supp}(\cdot)$ is defined in Definition 3.1. By considering the reality of computation, we treat $|u_j^k - f_j|$ as zero if it is small enough. Specifically, we define

$$\bar{\text{sup}}^\varepsilon(u) = \{j \in I_v : |u_j^k - f_j| > \varepsilon\},$$

and

$$\Gamma^k = \bar{\text{sup}}^\varepsilon(u^k), \quad \Gamma_c^k = I_v \setminus \bar{\text{sup}}^\varepsilon(u^k),$$

and change (11) into

$$\begin{cases} \min_{u \in \mathbb{R}^{N_v}} & \mathcal{F}_k(u) := \lambda \sum_{j \in \Gamma^k} |u_j - f_j|^p + \sum_{i \in I_\tau} |\tau_i| \|D_i u\|, \\ \text{s.t.} & u_j = f_j \quad \forall j \in \Gamma_c^k. \end{cases} \quad (12)$$

Directly solving (12) is difficult. The linearization is a common technique for nonlinear optimization. That is, the first-order Taylor approximation of some term around u^k , is employed to obtain an approximate objective function which is easy to solve. Specifically, for all $j \in \Gamma^k$, we have

$$|u_j - f_j|^p \approx |u_j^k - f_j|^p + p|u_j^k - f_j|^{p-1} (|u_j - f_j| - |u_j^k - f_j|). \quad (13)$$

For convenience, we define

$$w_j^k = p|u_j^k - f_j|^{p-1} \quad \forall j \in \Gamma^k. \quad (14)$$

Since the function $x \mapsto x^p$ is concave on $[0, +\infty)$, it follows that for all $j \in \Gamma^k$,

$$|u_j - f_j|^p \leq w_j^k |u_j - f_j| + (|u_j^k - f_j|^p - w_j^k |u_j^k - f_j|). \quad (15)$$

Substituting (13) into (12), deleting some constants and adding a proximal term, we obtain the following proximal linearization version of (12):

$$\begin{cases} \min_{u \in \mathbb{R}^{N_v}} & \mathcal{H}_k(u) := \lambda \sum_{j \in \Gamma^k} w_j^k |u_j - f_j| + \sum_{i \in I_\tau} |\tau_i| \|D_i u\| + \frac{\rho}{2} \|u - u^k\|^2, \\ \text{s.t.} & u_j = f_j \quad \forall j \in \Gamma_c^k. \end{cases} \quad (16)$$

The proximal term $\frac{\rho}{2} \|u - u^k\|^2$ is to increase the robustness of the nonconvex algorithm and is helpful in the global convergence. By (15), we can set ρ to be any positive scalar.

The whole procedure of the *proximal linearization method* (PLM) is summarized in Algorithm 1. Algorithm 1 can be extended to multichannel (e.g., color) image denoising.

Algorithm 1: proximal linearization method (PLM) for solving (6)

Input: $\Delta, \lambda, \varepsilon, f$
Initialize: $u^0, k = 0$
1 repeat
2 Update Γ^k, Γ_c^k
3 Update $w_j^{k+1}, j \in \Gamma^k$ by (14)
4 Solve u^{k+1} by (16)
5 $k \leftarrow k + 1$
6 until termination criteria met

Next, we introduce how to solve (16) by the alternating direction method of multipliers (ADMM).

3.2.1 Algorithm implementation

We reformulate $\mathcal{H}_k(u)$ in (16). The variable u is replaced by v to avoid confusion with the outer loops. We introduce two new variables: $y = (y_j)$, where $y_j \in \mathbb{R}$ and $j \in \Gamma^k$, and $z = (z_i)$, where $z_i \in \mathbb{R}^3$ and $i \in I_\tau$. Then (16) is reformulated as

$$\begin{aligned} \min_{v,y,z} \quad & \lambda \sum_{j \in \Gamma^k} w_j^k |y_j| + \sum_{i \in I_\tau} |\tau_i| \|z_i\| + \frac{\rho}{2} \|v - u^k\|^2, \\ \text{s.t.} \quad & y_j = v_j - f_j \quad \forall j \in \Gamma^k, \\ & z_i = D_i v \quad \forall i \in I_\tau, \\ & v_j = f_j \quad \forall j \in \Gamma_c^k. \end{aligned}$$

The augmented Lagrangian function for the above problem is defined as

$$\begin{aligned} \mathcal{L}(v, y, z; \eta, \mu) = & \lambda \sum_{j \in \Gamma^k} w_j^k |y_j| + \sum_{i \in I_\tau} |\tau_i| \|z_i\| + \frac{\rho}{2} \|v - u^k\|^2 \\ & + \sum_{j \in \Gamma^k} \eta_j (v_j - f_j - y_j) + \sum_{j \in \Gamma_c^k} \eta_j (v_j - f_j) + \sum_{i \in I_\tau} |\tau_i| \langle \mu_i, D_i v - z_i \rangle \\ & + \frac{\beta_1}{2} \sum_{j \in \Gamma^k} [y_j - (v_j - f_j)]^2 + \frac{\beta_1}{2} \sum_{j \in \Gamma_c^k} (v_j - f_j)^2 + \frac{\beta_2}{2} \sum_{i \in I_\tau} |\tau_i| \|z_i - D_i v\|^2, \end{aligned}$$

where $\beta_1, \beta_2 > 0, \eta_j \in \mathbb{R}, j \in I_v$ and $\mu_i \in \mathbb{R}^3, i \in I_\tau$ are Lagrange multipliers. Applying the ADMM yields Algorithm 2.

Algorithm 2: ADMM for solving (16)

Input: $u^k, \lambda, \rho, \beta_1, \beta_2$
Initialize: $v^0 = u^k, \eta^0 = 0, \mu^0 = 0, t = 0$

- 1 **repeat**
- 2 Compute (y^{t+1}, z^{t+1}) by solving

$$(y^{t+1}, z^{t+1}) \in \arg \min_{y,z} \mathcal{L}(v^t, y, z; \eta^t, \mu^t) \quad (17)$$
- 3 Compute v^{t+1} by solving

$$v^{t+1} \in \arg \min_v \mathcal{L}(v, y^{t+1}, z^{t+1}; \eta^t, \mu^t) \quad (18)$$
- 4 Update $\eta_j^{t+1} = \begin{cases} \eta_j^t + \beta_1 (v_j^{t+1} - f_j - y_j^{t+1}) & \forall j \in \Gamma^k \\ \eta_j^t + \beta_1 (v_j^{t+1} - f_j) & \forall j \in \Gamma_c^k \end{cases}$
- 5 Update $\mu_i^{t+1} = \mu_i^t + \beta_2 (D_i v^{t+1} - z_i^{t+1}) \quad \forall i \in I_\tau$
- 6 $t \leftarrow t + 1$
- 7 **until** termination criteria met

The two subproblems in the above algorithm are calculated as follows.

1. The (y, z) -subproblem (17): we can simplify (17) as

$$\begin{aligned} (y^{t+1}, z^{t+1}) \in \arg \min_{y,z} \left\{ \sum_{j \in \Gamma^k} \left(\lambda w_j^k |y_j| + \frac{\beta_1}{2} \left| y_j - \left(v_j^t - f_j + \frac{\eta_j^t}{\beta_1} \right) \right|^2 \right) \right. \\ \left. + \sum_{i \in I_\tau} |\tau_i| \left(\|z_i\| + \frac{\beta_2}{2} \left\| z_i - \left(D_i v^t + \frac{\mu_i^t}{\beta_2} \right) \right\|^2 \right) \right\}. \end{aligned}$$

The solution of above problem is given by the following one-dimensional and three-dimensional

shrinkage:

$$y_j^{t+1} = \max \left\{ \left| v_j^t - f_j + \frac{\eta_j^t}{\beta_1} \right| - \frac{\lambda w_j^k}{\beta_1}, 0 \right\} \circ \operatorname{sgn} \left(v_j^t - f_j + \frac{\eta_j^t}{\beta_1} \right) \quad \forall j \in \Gamma^k;$$

$$z_i^{t+1} = \max \left\{ \left\| D_i v^t + \frac{\mu_i^t}{\beta_2} \right\| - \frac{1}{\beta_2}, 0 \right\} \frac{D_i v^t + \frac{\mu_i^t}{\beta_2}}{\left\| D_i v^t + \frac{\mu_i^t}{\beta_2} \right\|} \quad \forall i \in I_\tau,$$

where the convention $0 \cdot (0/0) = 0$ is followed, and \circ denotes the pointwise product.

2. The v -subproblem (18): we introduce $\tilde{y} = (y_j)$ with $y_j = 0 \forall j \in \Gamma_c^k$, and define $\bar{y}^{t+1} = (y^{t+1}, \tilde{y}^{t+1})$. Then we can simplify (18) as

$$v^{t+1} \in \arg \min_v \left\{ \frac{\rho}{2} \|v - u^k\|^2 + \sum_{j \in I_v} \eta_j^t (v_j - f_j - \bar{y}_j^{t+1}) + \sum_{i \in I_\tau} |\tau_i| \langle \mu_i^t, D_i v - z_i^{t+1} \rangle + \frac{\beta_1}{2} \sum_{j \in I_v} [\bar{y}_j^{t+1} - (v_j - f_j)]^2 + \frac{\beta_2}{2} \sum_{i \in I_\tau} |\tau_i| \|z_i^{t+1} - D_i v\|^2 \right\}.$$

This is a least squares problem and the corresponding normal equation is

$$\left(\beta_2 \sum_{i \in I_\tau} |\tau_i| D_i^\top D_i + (\rho + \beta_1) I \right) v = \sum_{i \in I_\tau} |\tau_i| D_i^\top (\beta_2 z_i^{t+1} - \mu_i^t) + \beta_1 (\bar{y}^{t+1} + f) - \eta^t + \rho u^k$$

This is a sparse linear system and can be solved by various well-developed numerical packages.

4 Convergence analysis

In this section, we establish the global convergence of $\{u^k\}$, generated by Algorithm 1. Our proof is based on the Kurdyka-Łojasiewicz (KL) property of $\mathcal{F}(u)$. For examples of KL functions. For the reader's convenience, we provide some related facts and results on KL functions in Appendix B.

For the convergence analysis of nonconvex optimization, the KL property is pretty significant, which has drawn a great many of attention in recent years. For the development of the application of KL property in optimization theory, see [1–3, 7–9] and references therein. One can refer to [2, 3, 9], [25, Proposition 6], [36, section 3.3] for examples of KL functions. For this paper, $\mathcal{F}(u)$ is a KL function.

First, by (16), we have the following relationship:

$$\Gamma^{k+1} \subseteq \operatorname{supp}(u^{k+1}) \subseteq \Gamma^k \subseteq \operatorname{supp}(u^k). \quad (19)$$

Hence, $\{\#\Gamma^k\}$ is a non-increasing sequence. Since $\#\Gamma^k \in \{0, 1, \dots, N_v\}$, it follows that $\{\Gamma^k\}$ will converge within finite steps, i.e.,

$$\exists K, \text{ such that } \Gamma^k = \Gamma^K \quad \forall k \geq K. \quad (20)$$

We denote $\Gamma = \Gamma^K$ and $\Gamma_c = I_\tau \setminus \Gamma^K$. Then, when $k \geq K$, (16) becomes:

$$\begin{cases} \min_{u \in \mathbb{R}^{N_v}} & \bar{\mathcal{H}}_k(u) := \lambda \sum_{j \in \Gamma} w_j^k |u_j - f_j| + \sum_{i \in I_\tau} |\tau_i| \|D_i u\| + \frac{\rho}{2} \|u - u^k\|^2, \\ \text{s.t.} & u_j = f_j \quad \forall j \in \Gamma_c. \end{cases} \quad (21)$$

In order to eliminate the constraint of (21) for the convenience of convergence analysis, we define

$$\mathcal{C} := \{u \in \mathbb{R}^{N_v} : u_j = f_j \quad \forall j \in \Gamma_c\},$$

and the corresponding indicator function of \mathcal{C} as $\delta_{\mathcal{C}}$, where $\delta_{\mathcal{C}} : \mathbb{R}^{N_v} \rightarrow (-\infty, +\infty]$ is defined by

$$\delta_{\mathcal{C}}(u) = \begin{cases} 0 & \text{if } u \in \mathcal{C}, \\ +\infty & \text{otherwise.} \end{cases}$$

Then

$$\partial(\delta_{\mathcal{C}}(u)) = N_{\mathcal{C}}(u) = \begin{cases} \left\{ \sum_{j \in \Gamma_c} b_j e_j : b_j \in \mathbb{R} \right\} & \text{if } u \in \mathcal{C}, \\ \emptyset & \text{otherwise,} \end{cases}$$

where $N_{\mathcal{C}}(u)$ is the normal cone of \mathcal{C} at u . So (21) is equivalent to the following problem:

$$\min_{u \in \mathbb{R}^{N_v}} \bar{\mathcal{H}}_k^\delta(u) := \bar{\mathcal{H}}_k(u) + \delta_{\mathcal{C}}(u). \quad (22)$$

When $k \geq K$, $u^k \in \mathcal{C}$ and u^{k+1} solves $\bar{\mathcal{H}}_k^\delta(u)$ in (22).

In order to enable readers to better understand the proof, we review the definition of $\mathcal{F}(u)$, $\mathcal{F}_k(u)$ and $\mathcal{H}_k(u)$:

$$\begin{aligned} \mathcal{F}(u) &:= \lambda \sum_{j \in I_v} |u_j - f_j|^p + \sum_{i \in I_\tau} |\tau_i| \|D_i u\|, \\ \mathcal{F}_k(u) &:= \lambda \sum_{j \in \Gamma^k} |u_j - f_j|^p + \sum_{i \in I_\tau} |\tau_i| \|D_i u\|, \\ \mathcal{H}_k(u) &:= \lambda \sum_{j \in \Gamma^k} w_j^k |u_j - f_j| + \sum_{i \in I_\tau} |\tau_i| \|D_i u\| + \frac{\rho}{2} \|u - u^k\|^2. \end{aligned}$$

By the algorithm and (19), the following relation can be verified easily:

$$\mathcal{F}_k(u^{k+j}) = \mathcal{F}(u^{k+j}) \quad \forall k \geq 0, \forall j \geq 1. \quad (23)$$

Lemma 4.1. *Let $\{u^k\}$ be generated by Algorithm 1. Then, the objective function sequence $\{\mathcal{F}(u^k)\}$ satisfies*

$$\frac{\rho}{2} \|u^{k+1} - u^k\|^2 \leq \mathcal{F}(u^k) - \mathcal{F}(u^{k+1}) \quad \forall k \geq 0, \quad (24)$$

and $\{u^k\}$ is bounded.

Proof. According to (15), we have

$$\mathcal{F}_k(u) + \frac{\rho}{2} \|u - u^k\|^2 \leq \mathcal{H}_k(u) + \lambda \sum_{j \in \Gamma^k} (|u_j^k - f_j|^p - w_j^k |u_j^k - f_j|). \quad (25)$$

Letting $u = u^k$ yields that

$$\begin{aligned} \mathcal{H}_k(u^k) + \lambda \sum_{j \in \Gamma^k} (|u_j^k - f_j|^p - w_j^k |u_j^k - f_j|) &= \lambda \sum_{j \in \Gamma^k} |u_j^k - f_j|^p + \sum_{i \in I_\tau} |\tau_i| \|D_i u^k\| \\ &= \mathcal{F}(u^k). \end{aligned} \quad (26)$$

It follows that

$$\begin{aligned} &\mathcal{F}(u^{k+1}) + \frac{\rho}{2} \|u^{k+1} - u^k\|^2 \\ &\stackrel{(23)}{=} \mathcal{F}_k(u^{k+1}) + \frac{\rho}{2} \|u^{k+1} - u^k\|^2 \\ &\stackrel{(25)}{\leq} \mathcal{H}_k(u^{k+1}) + \lambda \sum_{j \in \Gamma^k} (|u_j^k - f_j|^p - w_j^k |u_j^k - f_j|) \\ &\leq \mathcal{H}_k(u^k) + \lambda \sum_{j \in \Gamma^k} (|u_j^k - f_j|^p - w_j^k |u_j^k - f_j|) \\ &\stackrel{(26)}{=} \mathcal{F}(u^k), \end{aligned}$$

which proves (24).

Combining (24) and the fact that $\mathcal{F}(u^k) \geq 0$ yields the convergence of $\{\mathcal{F}(u^k)\}$. Since $\mathcal{F}(u)$ is coercive, it follows that $\{u^k\}$ is bounded. \square

Next, we give a subdifferential lower bound for the iterates gap. Let $\{u^k\}$ be generated by Algorithm 1, when $k \geq K$, according to [38, Theorem 2.3], we have the following formula:

$$\partial \left(\lambda \sum_{j \in \Gamma_c} |u_j^k - f_j|^p \right) = \sum_{j \in \Gamma_c} (\ker e_j^\top)^\perp = \sum_{j \in \Gamma_c} \text{Im } e_j = N_{\mathcal{C}}(u^k). \quad (27)$$

Lemma 4.2. *Let $\{u^k\}$ be generated by Algorithm 1 and $k \geq K$. Then, there exists $\alpha^{k+1} \in \partial \mathcal{F}(u^{k+1})$ such that*

$$\|\alpha^{k+1}\| \leq \Lambda \|u^{k+1} - u^k\|, \quad (28)$$

where $\Lambda \geq 0$ is a constant.

Proof. By noting (27), direct calculation gives that

$$\partial \mathcal{F}(u^{k+1}) = \lambda \sum_{j \in \Gamma} w_j^{k+1} \text{sgn}(u_j^{k+1} - f_j) e_j + N_{\mathcal{C}}(u^{k+1}) + \partial \left(\sum_{i \in I_\tau} |\tau_i| \|D_i u^{k+1}\| \right). \quad (29)$$

Since u^{k+1} solves $\overline{\mathcal{H}}_k^\delta(u)$ in (22), by the first order optimality condition, we have

$$0 \in \partial \overline{\mathcal{H}}_k^\delta(u^{k+1}) = \partial \overline{\mathcal{H}}_k(u^{k+1}) + \partial \delta_{\mathcal{C}}(u^{k+1}).$$

Then, we have

$$-\lambda \sum_{j \in \Gamma} w_j^k \text{sgn}(u_j^{k+1} - f_j) e_j - \rho(u^{k+1} - u^k) \in \partial \left(\sum_{i \in I_\tau} |\tau_i| \|D_i u^{k+1}\| \right) + N_{\mathcal{C}}(u^{k+1}). \quad (30)$$

Therefore, combining (29) and (30) yields that

$$\alpha^{k+1} := \lambda \sum_{j \in \Gamma} (w_j^{k+1} - w_j^k) \text{sgn}(u_j^{k+1} - f_j) e_j - \rho(u^{k+1} - u^k) \in \partial \mathcal{F}(u^{k+1}).$$

By Algorithm 1, we have $|u_j^k - f_j| \geq \epsilon, \forall j \in \Gamma, \forall k \geq K$. Consider the function $x \mapsto x^{p-1}$. For any $x_2 > x_1 \geq \epsilon$, by the mean value theorem, there exists $x_0 \in (x_1, x_2)$ such that

$$|x_2^{p-1} - x_1^{p-1}| = (1-p)x_0^{p-2}|x_2 - x_1| \leq (1-p)\epsilon^{p-2}|x_2 - x_1|.$$

Then, by the definition (14), it follows that:

$$\begin{aligned} |w_j^{k+1} - w_j^k| &= p| |u_j^{k+1} - f_j|^{p-1} - |u_j^k - f_j|^{p-1} | \\ &\leq p(1-p)\epsilon^{p-2}|u_j^{k+1} - u_j^k| \leq p(1-p)\epsilon^{p-2} \|u^{k+1} - u^k\|. \end{aligned} \quad (31)$$

Therefore,

$$\begin{aligned} \|\alpha^{k+1}\| &\leq \lambda \sum_{j \in \Gamma} |w_j^{k+1} - w_j^k| + \rho \|u^{k+1} - u^k\| \\ &\stackrel{(31)}{\leq} (\lambda p(1-p)\epsilon^{p-2} N_v + \rho) \|u^{k+1} - u^k\| \\ &=: \Lambda \|u^{k+1} - u^k\|, \end{aligned}$$

where $\Lambda := \lambda p(1-p)\epsilon^{p-2} N_v + \rho$. □

Theorem 4.3. *Let $\{u^k\}$ be generated by Algorithm 1. Then $\{u^k\}$ converges to a critical point u^* of $\mathcal{F}(u)$.*

Proof. Since $\{u^k\}$ is bounded (see Lemma 4.1) and $\mathcal{F}(u)$ is continuous, there exists a subsequence $\{u^{k_j}\}$ and \hat{u} such that

$$u^{k_j} \rightarrow \hat{u} \text{ and } \mathcal{F}(u^{k_j}) \rightarrow \mathcal{F}(\hat{u}), \text{ as } j \rightarrow +\infty. \quad (32)$$

Combining (4.1) and (4.2), by [3, Theorem 2.9], the sequence $\{u^k\}$ converges to $u^* = \hat{u}$ globally, and u^* is a critical point of $\mathcal{F}(u)$. □

5 Experiments

In this section, we provide some numerical examples. The proposed algorithms are implemented with C++. All experiments are performed on Visual Studio 2019 on a desktop computer (Intel Core i7-8700 CPU @ 3.20GHz, 16G RAM). The peak signal-to-noise ratio (PSNR) is used to measure the quality of restored images. For grayscale images, the PSNR is defined as follows:

$$\text{PSNR} = 10 * \log_{10} \frac{N_v}{\|u - \underline{u}\|^2} \text{dB},$$

where N_v is the number of the vertices, \underline{u} is the original image, and u is the restored image. The PSNR of color images is defined similarly.

The stopping tolerance of PLM is set as

$$\frac{\|u^{k+1} - u^k\|}{\|u^{k+1}\|} < 10^{-6} \text{ or } \frac{\|\mathbf{u}^{k+1} - \mathbf{u}^k\|}{\|\mathbf{u}^{k+1}\|} < 10^{-6}.$$

The maximum iteration number is set to be 500. Generally, the choice of the initial point is crucial in nonconvex optimization. In this specific problem, if the initialization is distant from the original image, the support of the initial point may significantly differ from that of the original image. Considering that L_1 TV model can be viewed as a reliable convex approximation of L_p TV model, the solution obtained from the L_1 TV model is likely to remain close to the original image. Motivated by this observation, we use the result of the L_1 TV model, solved by ADMM [33], as the initialization u^0 or \mathbf{u}^0 .



Figure 4: Test images. From top left to bottom right: Ball, Bottle, Bunny, Horse, Mug and Flag.

We test six images shown in Figure 4, including four grayscale images and two color images. The sizes of the underlying meshes are shown in Table 1. Suppose the original grayscale image is \underline{u} . We impose some salt-and-pepper noise and obtain the observed image by

$$f = \underline{u} + n,$$

The noise of color image is imposed similarly.

5.1 Performance of PLM

In this subsection, we show the performance of the proposed method and compare it with the L_1 TV model solved by ADMM. We consider four levels of noise $\rho = 0.05, 0.10, 0.20, 0.30$ and $p = 0.1, 0.3, 0.5, 0.7, 0.9$. The noisy images with $\rho = 0.10$ are shown in Figure 5.

The comparison results are shown in Table 2, where all results are averaged over 10 trials for each case. We consider the PSNR. L_p TV outperforms L_1 TV for all cases. For most cases, the smaller p is, the higher PSNR is obtained. This is very natural, because a smaller p would enhance the sparsity of the data fitting

Table 1: Underlying meshes of test images

Image	Number of vertices	Number of triangles
Ball	40962	81920
Bottle	132300	264600
Horse	48480	96956
Mug	29664	59328
Bunny	34817	69630
Flag	163116	324500



Figure 5: Noisy images with zoomed regions, where the noise level is $\rho = 0.10$. The second (resp., fourth) column is the corresponding zoomed regions of the first (resp., third) column.

term of the solution. Since we consider recovering images corrupted by salt-and-pepper noise, L_p TV with a smaller p can yield better denoising results. In addition, it is observed that as the noise level increases, the performance of the L_p TV model degrades. This decline is attributed to the fact that, at higher noise levels, the requirement for sparse reconstruction in the data fitting term diminishes.

The visual comparison of some restorations is shown in Figure ?? and ?. All results are with respect to $\rho = 0.10$. From the zoomed regions, we can see the recovered results by the L_p TV model, especially by $p = 0.1$, have much better performances than those by the L_1 TV model.

6 Conclusions

In this paper, we consider recovering images corrupted by salt-and-pepper noise on surfaces with non-convex variational methods, i.e., proposing the L_p TV model on surfaces. From the perspective of sparse reconstruction, L_p TV model is suitable for salt-and-pepper noise removal. The lower bound property of the model is presented. Motivated by the lower bound property, we adopt proximal linearization method with the thresholding and support shrinking strategy. We establish the global convergence of the algorithm. Numerical examples are given to show good performance of the algorithm.

We adopt linear interpolation in this work. Linear interpolation is a basic way for interpolation and leads to a simple relationship between the image u and its gradient Du ; see (3). Based on this, we can prove the lower bound theory, i.e., Theorem 3.2. Moreover, the simple relationship between u and Du

Table 2: Comparison results of different methods. The running time is measured in seconds. The best results among L_pTV are highlighted in boldface.

Image	Noise level		L_1TV	L_pTV				
				$p = 0.9$	$p = 0.7$	$p = 0.5$	$p = 0.3$	$p = 0.1$
Ball	0.05	PSNR	-	-	-	-	-	-
		Time	-	-	-	-	-	-
	0.10	PSNR	-	-	-	-	-	-
		Time	-	-	-	-	-	-
0.20	PSNR	-	-	-	-	-	-	
	Time	-	-	-	-	-	-	
0.30	PSNR	-	-	-	-	-	-	
	Time	-	-	-	-	-	-	
Bottle	0.05	PSNR	-	-	-	-	-	-
		Time	-	-	-	-	-	-
	0.10	PSNR	-	-	-	-	-	-
		Time	-	-	-	-	-	-
0.20	PSNR	-	-	-	-	-	-	
	Time	-	-	-	-	-	-	
0.30	PSNR	-	-	-	-	-	-	
	Time	-	-	-	-	-	-	
Horse	0.05	PSNR	-	-	-	-	-	-
		Time	-	-	-	-	-	-
	0.10	PSNR	-	-	-	-	-	-
		Time	-	-	-	-	-	-
0.20	PSNR	-	-	-	-	-	-	
	Time	-	-	-	-	-	-	
0.30	PSNR	-	-	-	-	-	-	
	Time	-	-	-	-	-	-	
Mug	0.05	PSNR	35.61	36.90	38.75	39.39	39.65	39.71
		Time	16.8	36.6	32.9	24.5	23.1	21.6
	0.10	PSNR	34.21	34.69	36.15	36.65	37.01	37.19
		Time	16.4	34.5	38.3	28.6	26.0	32.68
0.20	PSNR	31.77	32.42	33.77	34.32	34.53	34.61	
	Time	18.6	247.7	36.7	50.5	37.2	36.0	
0.30	PSNR	30.46	31.10	31.95	32.41	32.68	32.74	
	Time	20.9	44.4	67.3	47.0	50.2	39.5	
Bunny	0.05	PSNR	-	-	-	-	-	-
		Time	-	-	-	-	-	-
	0.10	PSNR	-	-	-	-	-	-
		Time	-	-	-	-	-	-
0.20	PSNR	-	-	-	-	-	-	
	Time	-	-	-	-	-	-	
0.30	PSNR	-	-	-	-	-	-	
	Time	-	-	-	-	-	-	
Flag	0.05	PSNR	-	-	-	-	-	-
		Time	-	-	-	-	-	-
	0.10	PSNR	-	-	-	-	-	-
		Time	-	-	-	-	-	-
0.20	PSNR	-	-	-	-	-	-	
	Time	-	-	-	-	-	-	
0.30	PSNR	-	-	-	-	-	-	
	Time	-	-	-	-	-	-	

brings convenience for computation. If other interpolation methods are used, do we still have the lower bound theory and an efficient algorithm? This will be investigated in the future.

There are other image processing problems on surfaces, such as image segmentation [5, 12, 17, 29, 33], image decomposition [16, 34], and image inpainting [32]. We will discuss how to extend this work to these problems in the future.

A The subdifferential

Definition A.1. (Subdifferentials) Let $f : \mathbb{R}^n \rightarrow (-\infty, +\infty]$ be a proper, lower semicontinuous function. For a point $x \in \text{dom } f$,

(i) The regular subdifferential of f at x is defined as

$$\hat{\partial}f(x) = \left\{ u \in \mathbb{R}^n : \liminf_{y \rightarrow x, y \neq x} \frac{f(y) - f(x) - \langle u, y - x \rangle}{\|y - x\|_2} \geq 0 \right\};$$

(ii) The (limiting) subdifferential of f at x is defined as

$$\partial f(x) = \left\{ u \in \mathbb{R}^n : \exists x^k \rightarrow x, f(x^k) \rightarrow f(x), u^k \in \hat{\partial}f(x^k), u^k \rightarrow u \text{ as } k \rightarrow \infty \right\}.$$

Remark A.2. For any $x \in \text{dom } f$, $\hat{\partial}f(x) \subset \partial f(x)$. If f is differentiable at x , then $\hat{\partial}f(x) = \partial f(x) = \{\nabla f(x)\}$.

Remark A.3. A point x is a critical point of $f(x)$ if and only if $0 \in \partial f(x)$. If x^* is a local minimizer of $f(x)$, then $0 \in \partial f(x^*)$.

B KL functions

Definition B.1. (KL property and KL functions) The function $f : \mathbb{R}^n \rightarrow (-\infty, +\infty]$ has KL property at $\hat{x} \in \text{dom } \partial f$ if there exist $a \in (0, +\infty]$, a neighborhood U of \hat{x} , and a continuous concave function $\varphi : [0, a) \rightarrow [0, +\infty)$ such that

(i) $\varphi(0) = 0$;

(ii) φ is C^1 on $(0, a)$;

(iii) for all $s \in (0, a)$, $\varphi'(s) > 0$;

(iv) for all $x \in U \cap \{f(\hat{x}) < f(x) < f(\hat{x}) + a\}$, the Kurdyka-Łojasiewicz inequality holds:

$$\varphi'(f(x) - f(\hat{x})) \text{dist}(0, \partial f(x)) \geq 1.$$

If the function f satisfies the KL property at each point of $\text{dom } \partial f$, f is called a KL function.

References

- [1] H. Attouch and J. Bolte. On the convergence of the proximal algorithm for nonsmooth functions involving analytic features. *Mathematical Programming*, 116(1):5–16, 2009.
- [2] H. Attouch, J. Bolte, P. Redont, and A. Soubeyran. Proximal alternating minimization and projection methods for nonconvex problems: An approach based on the Kurdyka-Łojasiewicz inequality. *Mathematics of Operations Research*, 35(2):438–457, 2010.
- [3] H. Attouch, J. Bolte, and B. F. Svaiter. Convergence of descent methods for semi-algebraic and tame problems: proximal algorithms, forward-backward splitting, and regularized Gauss-Seidel methods. *Mathematical Programming*, 137(1-2):91–129, 2013.
- [4] C. L. Bajaj and G. Xu. Anisotropic diffusion of surfaces and functions on surfaces. *ACM Transactions on Graphics*, 22(1):4–32, 2003.
- [5] H. Benninghoff and H. Garcke. Segmentation and restoration of images on surfaces by parametric active contours with topology changes. *Journal of Mathematical Imaging and Vision*, 55(1):105–124, 2016.
- [6] W. Bian and X. Chen. Linearly constrained non-Lipschitz optimization for image restoration. *SIAM Journal on Imaging Sciences*, 8(4):2294–2322, 2015.

- [7] J. Bolte, A. Daniilidis, and A. Lewis. The Łojasiewicz inequality for nonsmooth subanalytic functions with applications to subgradient dynamical systems. *SIAM Journal on Optimization*, 17(4):1205–1223, 2007.
- [8] J. Bolte, A. Daniilidis, A. Lewis, and M. Shiota. Clarke subgradients of stratifiable functions. *SIAM Journal on Optimization*, 18(2):556–572, 2007.
- [9] J. Bolte, S. Sabach, and M. Teboulle. Proximal alternating linearized minimization for nonconvex and nonsmooth problems. *Mathematical Programming*, 146(1-2):459–494, 2014.
- [10] E. J. Candes, M. B. Wakin, and S. P. Boyd. Enhancing sparsity by reweighted ℓ_1 minimization. *Journal of Fourier Analysis and Applications*, 14(5):877–905, 2008.
- [11] T. F. Chan and S. Esedoglu. Aspects of total variation regularized L^1 function approximation. *SIAM Journal on Applied Mathematics*, 65(5):1817–1837, 2005.
- [12] A. Delaunoy, K. Fundana, E. Prados, and A. Heyden. Convex multi-region segmentation on manifolds. In *Computer Vision, 2009 IEEE 12th International Conference on*, pages 662–669. IEEE, 2009.
- [13] M. Herrmann, R. Herzog, H. Kröner, S. Schmidt, and J. Vidal. Analysis and an interior-point approach for TV image reconstruction problems on smooth surfaces. *SIAM Journal on Imaging Sciences*, 11(2):889–922, 2018.
- [14] M. Hintermüller and T. Wu. Nonconvex TV^q -models in image restoration: Analysis and a trust-region regularization-based superlinearly convergent solver. *SIAM Journal on Imaging Sciences*, 6(3):1385–1415, 2013.
- [15] A. N. Hirani. *Discrete exterior calculus*. California Institute of Technology, 2003.
- [16] M. Huska, A. Lanza, S. Morigi, and I. Selesnick. A convex-nonconvex variational method for the additive decomposition of functions on surfaces. *Inverse Problems*, 35(12):124008, 2019.
- [17] M. Huska, A. Lanza, S. Morigi, and F. Sgallari. Convex non-convex segmentation of scalar fields over arbitrary triangulated surfaces. *Journal of Computational and Applied Mathematics*, 2018.
- [18] J. John and M. Wilschy. Image processing techniques for surface characterization of nanostructures. In *International Conference on Circuit, Power and Computing Technologies*, pages 1–6, 2016.
- [19] M.-J. Lai, Y. Xu, and W. Yin. Improved iteratively reweighted least squares for unconstrained smoothed ℓ_q minimization. *SIAM Journal on Numerical Analysis*, 51(2):927–957, 2013.
- [20] R. Lai and T. F. Chan. A framework for intrinsic image processing on surfaces. *Computer Vision and Image Understanding*, 115(12):1647–1661, 2011.
- [21] Y. Liu, C. Wu, and C. Zeng. Non-Lipschitz variational models and their iteratively reweighted least squares algorithms for image denoising on surfaces. *SIAM Journal on Imaging Sciences*, 17(2):1255–1283, 2024.
- [22] M. Nikolova. Analysis of the recovery of edges in images and signals by minimizing nonconvex regularized least-squares. *Multiscale Modeling & Simulation*, 4(3):960–991, 2005.
- [23] M. Nikolova, M. K. Ng, and C. P. Tam. On ℓ_1 data fitting and concave regularization for image recovery. *SIAM Journal on Scientific Computing*, 35(1):A397–A430, 2013.
- [24] M. Nikolova, M. K. Ng, S. Zhang, and W.-K. Ching. Efficient reconstruction of piecewise constant images using nonsmooth nonconvex minimization. *SIAM Journal on Imaging Sciences*, 1(1):2–25, 2008.
- [25] P. Ochs, A. Dosovitskiy, T. Brox, and T. Pock. On iteratively reweighted algorithms for nonsmooth nonconvex optimization in computer vision. *SIAM Journal on Imaging Sciences*, 8(1):331–372, 2015.
- [26] R. T. Rockafellar and R. J.-B. Wets. *Variational Analysis*, volume 317. Springer Science & Business Media, 2009.
- [27] L. I. Rudin, S. Osher, and E. Fatemi. Nonlinear total variation based noise removal algorithms. *Physica D: Nonlinear Phenomena*, 60(1):259–268, 1992.
- [28] Y. Shi, R. Lai, and A. W. Toga. Cortical surface reconstruction via unified Reeb analysis of geometric and topological outliers in magnetic resonance images. *IEEE Transactions on Medical Imaging*, 32(3):511–530, 2013.

- [29] A. Spira and R. Kimmel. Segmentation of images painted on parametric manifolds. In *Signal Processing Conference, 2005 13th European*, pages 1–4. IEEE, 2005.
- [30] C. Wu, J. Deng, and F. Chen. Diffusion equations over arbitrary triangulated surfaces for filtering and texture applications. *IEEE Transactions on Visualization and Computer Graphics*, 14(3):666–679, 2008.
- [31] C. Wu, J. Deng, F. Chen, and X. Tai. Scale-space analysis of discrete filtering over arbitrary triangulated surfaces. *SIAM Journal on Imaging Sciences*, 2(2):670–709, 2009.
- [32] C. Wu, J. Deng, W. Zhu, and F. Chen. Inpainting images on implicit surfaces. In *Pacific Graphics*, pages 142–144, 2005.
- [33] C. Wu, J. Zhang, Y. Duan, and X.-C. Tai. Augmented Lagrangian method for total variation based image restoration and segmentation over triangulated surfaces. *Journal of Scientific Computing*, 50(1):145–166, 2012.
- [34] X. Wu, J. Zheng, C. Wu, and Y. Cai. Variational structure–texture image decomposition on manifolds. *Signal Processing*, 93(7):1773–1784, 2013.
- [35] J. Yang, Y. Zhang, and W. Yin. An efficient TVL1 algorithm for deblurring multichannel images corrupted by impulsive noise. *SIAM Journal on Scientific Computing*, 31(4):2842–2865, 2009.
- [36] C. Zeng, R. Jia, and C. Wu. An iterative support shrinking algorithm for non-Lipschitz optimization in image restoration. *Journal of Mathematical Imaging and Vision*, 61(1):122–139, 2019.
- [37] C. Zeng and C. Wu. On the edge recovery property of nonconvex nonsmooth regularization in image restoration. *SIAM Journal on Numerical Analysis*, 56(2):1168–1182, 2018.
- [38] Z. Zheng, M. Ng, and C. Wu. A globally convergent algorithm for a class of gradient compounded non-Lipschitz models applied to non-additive noise removal. *Inverse Problems*, 36(12):125017, 2020.